

RSC Mechanochemistry

Accepted Manuscript

This article can be cited before page numbers have been issued, to do this please use: C. L. Rom, A. Shotwell, S. Combs, A. Peters, L. Borgia, H. Martin, M. P. Moghadasnia, J. Neilson and A. E. Maughan, *RSC Mechanochem.*, 2026, DOI: 10.1039/D5MR00114E.



This is an Accepted Manuscript, which has been through the Royal Society of Chemistry peer review process and has been accepted for publication.

Accepted Manuscripts are published online shortly after acceptance, before technical editing, formatting and proof reading. Using this free service, authors can make their results available to the community, in citable form, before we publish the edited article. We will replace this Accepted Manuscript with the edited and formatted Advance Article as soon as it is available.

You can find more information about Accepted Manuscripts in the [Information for Authors](#).

Please note that technical editing may introduce minor changes to the text and/or graphics, which may alter content. The journal's standard [Terms & Conditions](#) and the [Ethical guidelines](#) still apply. In no event shall the Royal Society of Chemistry be held responsible for any errors or omissions in this Accepted Manuscript or any consequences arising from the use of any information it contains.

Cite this: DOI: 00.0000/xxxxxxxxxx

Ball milling enables phase-pure synthesis of a temperature sensitive ternary chloride, MgZrCl₆[†]Christopher L. Rom,^{*a} Austin M. Shotwell,^b Sinclair R. Combs,^b Autumn Peters,^c Lauren Borgia,^c Hannah M. Martin,^b Michael P. Moghadasnia,^b James R. Neilson,^{c,d} and Annalise E. Maughan^{*a,b}Received Date
Accepted Date

DOI: 00.0000/xxxxxxxxxx

Ball milling is a powerful synthetic tool for discovering new inorganic materials. Inspired by the high ionic conductivity in Li₂ZrCl₆ synthesized via mechanochemistry, we synthesized MgZrCl₆ with a similar method. High resolution synchrotron X-ray diffraction shows that MgZrCl₆ is poorly crystalline after ball milling, but crystallizes in a layered hexagonal structure (*P* $\bar{3}$ 1*c*) after heat treatment. In situ synchrotron X-ray diffraction and differential scanning calorimetry measurements reveal a narrow temperature window around 400 °C in which crystallization occurs. Pair distribution function analysis shows 2D sheets of MgZrCl₆ form after milling, with heating driving 3D crystallization. Raman spectroscopy also shows evidence of Zr-Cl octahedral coordination familiar to MgZrCl₆ after milling. Electrochemical impedance spectroscopy does not reveal ionic conductivity in MgZrCl₆ (limit of detection ca. 1.4×10^{-8} S/cm). In addition to supporting existing design rules for Mg-based solid electrolytes, this work shows the power of ball milling to synthesize temperature-sensitive inorganic compounds with high yield.

Introduction

While traditional solid-state synthesis techniques rely on high temperatures to drive solid-state diffusion, ball milling can drive inter-diffusion between solids at low temperatures. Therefore, the mechanochemical technique can be an atomically efficient process for synthesizing materials ranging from halide perovskites

for optoelectronic applications^{9,10} to solid electrolytes for batteries. Leading Li- and Na-based solid electrolytes, such as sulfide argyrodites,¹¹ ternary chlorides,¹² and oxychlorides,¹³ have been synthesized via ball milling. However, solid-state Mg electrolytes remain a nascent research topic¹⁴ which ball milling may expand.

Chlorides have emerged as a promising class of materials for Li⁺ solid electrolytes owing to their high ionic conductivity, low electronic conductivity, and high oxidative stability,¹⁵ but are underexplored for Mg²⁺ conductivity. To the best of our knowledge, MgM₂Cl₈ phases (*M* = Al, Ga) are the only chlorides that have been studied as Mg²⁺ ion conductors.^{16,17} They were synthesized via high-temperature solid-state techniques and exhibit ionic conductivity ca. 10^{-6} to 10^{-5} S/cm at 127 °C. Although these few examples underperform leading selenide¹⁸ and borohydride¹⁹ materials, further exploration of chlorides is warranted. Solid state synthesis methods yielded chlorides with low-to-moderate Li⁺ ion conductors in the 1990's, but the ball milling synthesis of Li₃YCl₆ produced a fast ion conductor in 2018 and started a renaissance of chloride-based solid electrolytes.^{15,20}

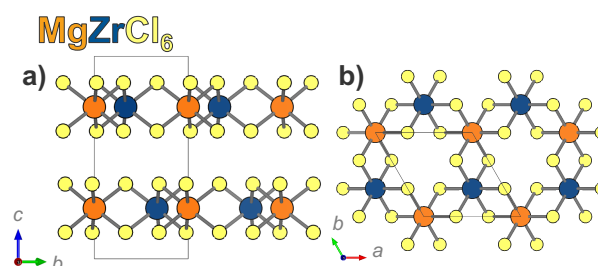


Fig. 1 a) View of the MgZrCl₆ structure down the *a* axis. b) View of one layer of the structure looking down the *c* axis.

MgZrCl₆ has a layered structure that may be conducive to Mg²⁺ mobility (Figure 1), but it has not been studied for this property. We first noticed this phase as an intermediate in the

^a Materials Science Center, National Laboratory of the Rockies, Golden, CO, 80401, USA. E-mail: christopher.rom@nrel.gov

^b Department of Chemistry, Colorado School of Mines Golden, CO, 80401, USA. Email: amaughan@mines.edu

^c Department of Chemistry, Colorado State University, Fort Collins, CO, 80523, USA

^d School of Materials Science & Engineering, Colorado State University, Fort Collins, CO, 80523, USA

[†] Supplementary Information available: Experimental methods, PXRD analysis, Raman spectroscopy results, Bond Valence Site Analysis, and additional references. ¹⁻⁸ See DOI: 00.0000/00000000.



metathesis reaction: $2\text{Mg}_2\text{NCl} + \text{ZrCl}_4 \longrightarrow \text{MgZrN}_2 + 3\text{MgCl}_2$.²¹ A 2014 report by Salyulev and Vovkotrub noted that MgZrCl_6 was previously studied to better understand corrosion in chloride-based metallurgical processes,²² and they referenced synthesis literature for these phases from the 1990's.^{23,24} We have not been able to access these original synthesis reports, but the 2014 report suggests that MgZrCl_6 was synthesized using elevated ZrCl_4 vapor pressures (ca. 22–59 atm) and in narrow temperature ranges (ca. 450–500 °C).²² Given the volatility of ZrCl_4 (sublimation point, 331 °C), we hypothesized that mechanochemistry may provide a route to phase pure MgZrCl_6 .

Results and Discussion

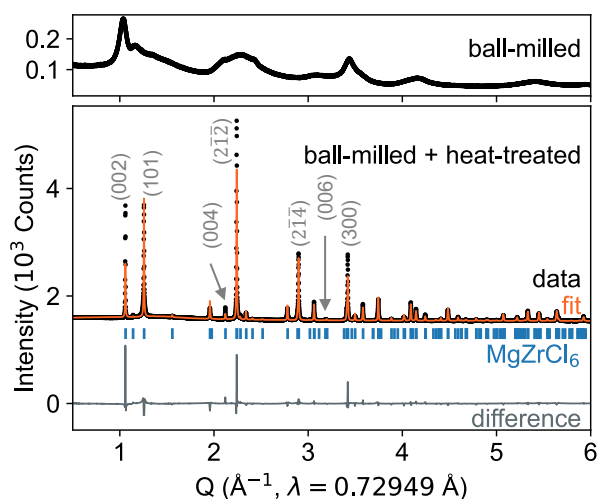


Fig. 2 Synchrotron PXRD of MgZrCl_6 prepared by ball milling and the sample after heat treatment at 350 °C for 2 h in a sealed ampule.

High-resolution synchrotron powder X-ray diffraction (PXRD) shows that 10 h of high-energy ball milling (BM) of $\text{MgCl}_2 + \text{ZrCl}_4$ produced poorly crystalline MgZrCl_6 (Figure 2). ZrO_2 jars and balls were used for milling (more details in ESI). Subsequent heat treatment (BM+HT) crystallizes MgZrCl_6 in space group $P\bar{3}1c$ ($a = 6.35975(3)$ Å and $c = 11.8428(1)$ Å), isostructural with FeZrCl_6 (Inorganic Crystal Structure Database Col. Code 39666).³ Ball milling was crucial for the synthesis of phase pure MgZrCl_6 , as hand-ground mixtures of reagents only reacted partially (Figures S1, S2).

The crystal structure of MgZrCl_6 (BM+HT) consists of layers stacked along the c direction, with each layer containing edge-sharing $[\text{MgCl}_6]$ and $[\text{ZrCl}_6]$ octahedra. Within the layer, 2/3 of the octahedral sites are occupied with an alternating pattern of Mg^{2+} and Zr^{4+} , while the remaining 1/3 of octahedral sites are vacant. Consequently, each Mg^{2+} is neighbored by three Zr^{4+} and three vacant octahedra. The chloride anions form a hexagonal close-packed arrangement with a van der Waals gap between the layers. We note three significant peaks in the difference trace, indicating that the (002), (212), and (300) Bragg peaks are under-fit by our model. Our attempts to improve our model with stacking faults, anisotropic peak broadening, and cation-disorder, were unsuccessful. We also considered a structural model based

on TiYbI_6 (ICSD Col. Code 138835), which also crystallizes in the $P\bar{3}1c$ space group but with different atomic coordinates: that model was substantially worse. It is possible for cations to disorder into van der Waals gap,²⁵ but our attempts to refine electron density in inter-layer sites did not substantially improve the fit. Single crystal diffraction measurements may be needed to more precisely determine the structure.

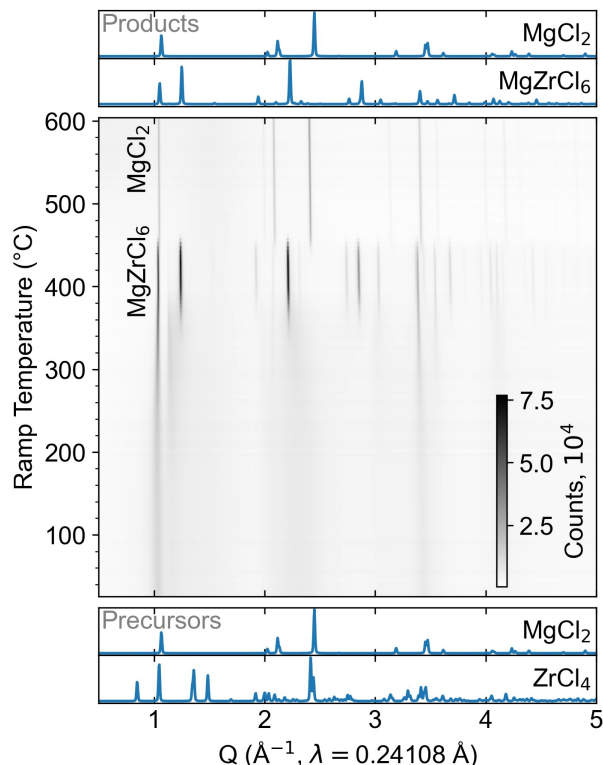


Fig. 3 *In situ* synchrotron PXRD of a BM mixture of $\text{MgCl}_2 + \text{ZrCl}_4$ upon heating at +10 °C/min. Simulated reference patterns for the precursors and products are shown at the bottom and top, respectively.

In situ synchrotron PXRD shows the crystallization and decomposition pathway for MgZrCl_6 from ball milled precursors (Figure 3). Broad peaks are present at room temperature, indicating that ball milling resulted in a poorly crystalline ternary phase. At 340 °C, the broad peaks of the initial phase sharpen, and additional reflections appear as MgZrCl_6 rapidly crystallizes. At 460 °C, the MgZrCl_6 peaks abruptly disappear, leaving behind only MgCl_2 . This change shows that MgZrCl_6 has limited thermal stability, decomposing to MgCl_2 (s) and ZrCl_4 (g) at moderate temperatures. These *in situ* findings are consistent with our *ex situ* results (Figure S1) and with differential scanning calorimetry (DSC) measurements (Figure S9).

Pair distribution function (PDF) analysis of X-ray total scattering data suggest that BM MgZrCl_6 has a similar local structure to BM+HT MgZrCl_6 (Figure 4). The BM+HT sample exhibits short and long range pair correlations that are well fit by the $P\bar{3}1c$ MgZrCl_6 model (Figure 4a). The PDF of the ball milled sample reveals significantly attenuated pair correlations beyond $r \approx 6$ Å. Furthermore, the bulk crystal structure does not fit these data well beyond $r \approx 4$ Å, particularly at distances corresponding to the in-



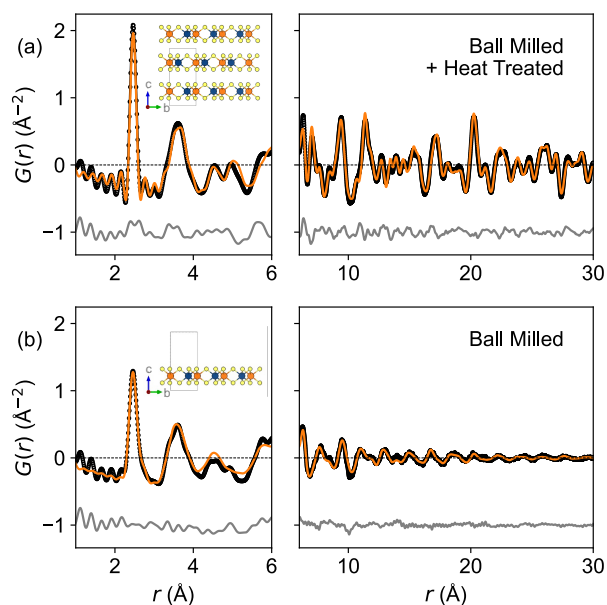


Fig. 4 PDF of X-ray total scattering data from (a) BM+HT samples and (b) BM of MgZrCl_6 . Data in black, fit in orange, difference in gray (offset vertically by 1 \AA^{-2}). Insets show structural models.

terlayer separations (Figure ??). Instead, a composite model with a single layer of MgZrCl_6 as implemented in PDFgui²⁶ following Ref. 27 with a spherical truncation diameter of $50(30) \text{ \AA}$, provides the best fit to the data (Figure 4b). A similar result was observed via PDF for the initial stages of FeS nanosheet growth from solution.²⁸ This suggests that ball milling induces formation of MgZrCl_6 sheets with octahedral coordination and some Mg-Zr ordering, but annealing is necessary to induce extended ordering. Although poorly-crystalline milled materials “age” in some cases,²⁹ we do not observe this behavior in MgZrCl_6 . Laboratory PXRD data of the same ball-milled material collected ~ 3 years after the synchrotron powder X-ray diffraction data (Figure 2) exhibits similar broadened features (Figure S10).

Raman spectroscopy shows that the BM MgZrCl_6 has structural motifs that are conserved upon crystallization (Figure 5). The Raman spectrum of BM+HT MgZrCl_6 has peaks at 327 cm^{-1} , 177 cm^{-1} , and 116 cm^{-1} . Similar peaks also appear in the spectrum for the BM MgZrCl_6 . While we do not precisely assign these vibrational modes, these shared peaks suggest that structural motifs of the crystallized MgZrCl_6 are already present in the poorly crystalline material produced by the ball milling step, consistent with PDF analysis. The BM MgZrCl_6 spectrum also has broad peaks at 410 cm^{-1} , 232 cm^{-1} , and 135 cm^{-1} that roughly correspond to peaks from the binary halide precursors, suggesting that mechanochemical conversion to MgZrCl_6 is incomplete (10 h milling time). In contrast, the spectrum from the hand-ground sample of $\text{MgCl}_2 + \text{ZrCl}_4$ is merely a linear combination of the precursor spectra. These data show that ball milling initiates formation of the MgZrCl_6 phase, which crystallizes on heating.

Given the open framework of MgZrCl_6 with an ordered arrangement of vacant octahedra within layers and a van der Waals gap between layers (Figure 1), we hypothesized that Mg^{2+} may

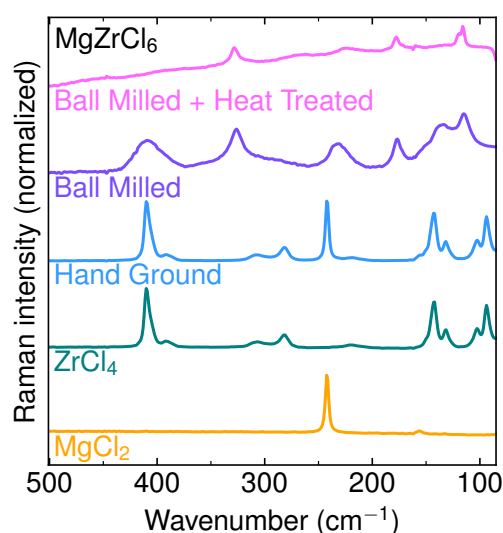


Fig. 5 Background-subtracted Raman spectra of the crystallized MgZrCl_6 (BM+HT) and poorly-crystalline ball milled MgZrCl_6 compared with the hand-ground precursor mix $\text{MgCl}_2 + \text{ZrCl}_4$ and the binary precursors. Raw spectra are shown in Figure S4.

be mobile in the structure. We performed AC electrochemical impedance spectroscopy (EIS) in a two-electrode configuration up to $95 \text{ }^\circ\text{C}$. The BM and BM+HT MgZrCl_6 did not exhibit charge transport behavior (Figures ??, ??). Rather, the materials show capacitive behavior consistent with a dielectric. Given the limit of detection for the measurement (approximately $4 \text{ M}\Omega$) along with the pellet dimensions (0.71 mm thick, 1.27 cm^2 cross-sectional area), we can rule out ionic conductivity above approximately $1.4 \times 10^{-8} \text{ S/cm}$. We attempted aliovalent substitution of Nb^{5+} into MgZrCl_6 in hopes of boosting ionic conductivity (Figure ??), but the more volatile NbCl_5 separated from the pellet during annealing and was not incorporated into the structure.

The negligible ionic conductivity of this phase is consistent with design rules for multivalent ion conductors described in prior literature. Rong et al. proposed that Mg^{2+} mobility may be favorable in structures where Mg^{2+} ions sit in energetically-disfavored sites (i.e., tetrahedra).⁷ In MgZrCl_6 , Mg^{2+} occupies an octahedral site, which is more stable and thus less prone to hopping. Iton and See also noted that repulsive forces increase when a mobile ion moves through a site that is face-sharing with a site occupied by a highly-charged cation.⁸ The Zr^{4+} sites in MgZrCl_6 are face-sharing with $2/3$ of the octahedral holes within the Van der Waals gap, inhibiting Mg^{2+} mobility within that layer. Bond Valence Site Energy calculations suggest the lowest migration barrier in MgZrCl_6 is 0.86 eV for interlayer hopping (Figure S8). This value is higher than the 0.6 eV cutoff used for prior theoretical work screening for Mg^{2+} ion conductors.⁶ Our findings therefore further validate the design rules posed in these prior works.

Although MgZrCl_6 proved not to be an Mg^{2+} ion conductor, the synthetic approach may be useful for yielding phase-pure solids that include volatile precursors. Our preliminary work in this Mg-Zr-Cl system motivates further study into other compositions that may be stabilized through mechanochemical meth-



ods. In this case, $ZrCl_4$ sublimates at 330 °C, but ball milling can trap it within the $MgZrCl_6$ framework, allowing for subsequent heat treatment at 350 °C to crystallize the ternary without vapor loss. Many other chlorides also have low boiling or sublimation points, such as $TiCl_4$ (boils at 136 °C), $AlCl_3$ (sublimates at 180 °C), and $NbCl_5$ (boils at 247 °C). Similarly, many bromides and iodides boil, sublime, or decompose at relatively low temperatures. The ball milling approach here may enable the synthesis of other temperature-sensitive halides.

Author Contributions

C.L.R. and A.M.S. contributed equally.

C.L.R.- Conceptualization, Formal Analysis, Investigation, Visualization, Writing – Original Draft. A.M.S.- Formal Analysis, Investigation, Visualization S.R.C.- Formal Analysis. A.P.- Investigation. L.B.- Investigation. H.M.M.- Investigation. M.P.M.- Investigation. J.R.N.- Formal Analysis. A.E.M.- Formal Analysis, Funding Acquisition. All authors edited the manuscript.

Conflicts of interest

There are no conflicts to declare.

Data availability

Crystallographic data on $MgZrCl_6$ are available at the Cambridge Crystallographic Data Centre (CCDC Deposition number 2421152). Data for this article, including diffraction patterns, PDF data, and Raman spectra, are available at FigShare at <https://doi.org/10.6084/m9.figshare.c.8023465>. Additional data supporting this article have been included as part of the ESI.†

Acknowledgments

This work was authored by the National Laboratory of the Rockies for the U.S. Department of Energy (DOE), operated under Contract No. DE-AC36-08GO28308. C.L.R. and A.E.M. acknowledge support from the Laboratory Directed Research and Development (LDRD) program at NLR. Thanks to Sita Dugu for helpful discussions of Raman spectroscopy. Use of the Advanced Photon Source at Argonne National Laboratory was supported by the U.S. Department of Energy, Office of Science, Office of Basic Energy Sciences, under Contract no. DE-AC02-06CH11357. Use of the Stanford Synchrotron Radiation Lightsource, SLAC National Accelerator Laboratory, is supported by the U.S. Department of Energy, Office of Science, Office of Basic Energy Sciences under Contract no. DE-AC02-76SF00515. The views expressed in the article do not necessarily represent the views of the DOE or the U.S. Government.

Notes and references

- C. L. Rom, P. Yox, A. M. Cardoza, R. W. Smaha, M. Q. Phan, T. R. Martin and A. E. Maughan, *Chem. Mater.*, 2024, **36**, 7283–7291.
- K. H. Stone, M. R. Cosby, N. A. Strange, V. Thampy, R. C. Walroth and C. Troxel Jr, *J. Appl. Crystallogr.*, 2023, **56**, 1480–1484.
- S. Troyanov, B. Kharisov and S. Berdonosov, *Zhurnal Neorganicheskoy Khimii*, 1992, **37**, 2424–2429.
- P. J. Chupas, K. W. Chapman, C. Kurtz, J. C. Hanson, P. L. Lee and C. P. Grey, *J. Appl. Crystallogr.*, 2008, **41**, 822–824.
- P. Juhás, T. Davis, C. L. Farrow and S. J. Billinge, *Appl. Crystallogr.*, 2013, **46**, 560–566.
- T. Chen, G. Sai Gautam and P. Canepa, *Chem. Mater.*, 2019, **31**, 8087–8099.
- Z. Rong, R. Malik, P. Canepa, G. Sai Gautam, M. Liu, A. Jain, K. Persson and G. Ceder, *Chem. Mater.*, 2015, **27**, 6016–6021.
- Z. W. Iton and K. A. See, *Chem. Mater.*, 2022, **34**, 881–898.
- F. Palazon, Y. El Ajjouri and H. J. Bolink, *Adv. Energy Mater.*, 2020, **10**, 1902499.
- D. Ceriotti, P. Marziani, F. M. Scesa, A. Collorà, C. L. Bianchi, L. Magagnin and M. Sansotera, *RSC Mechanochem.*, 2024, **1**, 520–530.
- S. Boulineau, M. Courty, J.-M. Tarascon and V. Viallet, *Solid State Ionics*, 2012, **221**, 1–5.
- H. Kwak, D. Han, J. Lyoo, J. Park, S. H. Jung, Y. Han, G. Kwon, H. Kim, S.-T. Hong, K.-W. Nam *et al.*, *Adv. Energy Mater.*, 2021, **11**, 2003190.
- T. Zhao, B. Samanta, X. M. de Irujo-Labalde, G. Whang, N. Yadav, M. A. Kraft, P. Adelmhelm, M. R. Hansen and W. G. Zeier, *ACS Mater. Lett.*, 2024, **6**, 3683–3689.
- P. W. Jaschin, Y. Gao, Y. Li and S.-H. Bo, *J. Mater. Chem. A*, 2020, **8**, 2875–2897.
- S. R. Combs, P. K. Todd, P. Gorai and A. E. Maughan, *J. Electrochem. Soc.*, 2022, **169**, 040551.
- Y. Tomita, R. Saito, A. Nagata, Y. Yamane and Y. Kohno, *Energies*, 2020, **13**, 6687.
- Y. Tomita, R. Saito, M. Morishita, Y. Yamane and Y. Kohno, *Solid State Ionics*, 2021, **361**, 115566.
- P. Canepa, S.-H. Bo, G. Sai Gautam, B. Key, W. D. Richards, T. Shi, Y. Tian, Y. Wang, J. Li and G. Ceder, *Nature Commun.*, 2017, **8**, 1759.
- E. Roedern, R.-S. Kühnel, A. Remhof and C. Battaglia, *Sci. Rep.*, 2017, **7**, 46189.
- T. Asano, A. Sakai, S. Ouchi, M. Sakaida, A. Miyazaki and S. Hasegawa, *Adv. Mater.*, 2018, **30**, 1803075.
- C. L. Rom, M. J. Fallon, A. Wustrow, A. L. Prieto and J. R. Neilson, *Chem. Mater.*, 2021, **33**, 5345–5354.
- A. Салюлев, АБ and Вовкотруб, ЭГ, (*Salyulev and E. Vovkotrub, Расплавы (Melts)*, 2014, 71–77.
- A. Salyulev, E. Vovkotrub and V. Strekalovsky, International Conference on Raman Spectroscopy, 1998, pp. 714–715.
- Салюлев, АБ and Вовкотруб, ЭГ and Стрекаловский, ВН, Ж. неорган. химии (*translation: J. Inorganic Chemistry*), 1990, **35**, 902.
- H. C. Mandujano, T. Li, P. Y. Zavalij and E. E. Rodriguez, *Chem. Mater.*, 2024, **36**, 5172–5183.
- C. L. Farrow, P. Juhás, J. W. Liu, D. Bryndin, E. S. Bozin, J. Bloch, T. Proffen and S. J. L. Billinge, *J. Phys.: Condens. Matter*, 2007, **19**, 335219.
- Z. Chen, M. L. Beauvais and K. W. Chapman, *J. Appl. Crystallogr.*, 2023, **56**, 328–337.
- M. L. Beauvais, P. J. Chupas, D. O’Nolan, J. B. Parise and K. W.



- Chapman, *ACS Mater. Lett.*, 2021, **3**, 698–703.
29 C. Mottillo and T. Friščić, *Molecules*, 2017, **22**, 144.

Open Access Article. Published on 13 April 2026. Downloaded on 4/14/2026 11:17:49 PM.
This article is licensed under a Creative Commons Attribution 3.0 Unported Licence.



Crystallographic data on MgZrCl₆ are available at the Cambridge Crystallographic Data Centre (CCDC Deposition number 2421152). Data for this article, including diffraction patterns, PDF data, and Raman spectra, are available at FigShare at <https://doi.org/10.6084/m9.figshare.c.8023465>. Additional data supporting this article have been included as part of the ESI.†

